공학석사 학위논문

An effect of AC electrothermal flow on a carbon nanotube network based biosensor

AC electrothermal flow가 탄소나노튜브 네트워크 기반 바이오센서에 주는 효과

2017 년 2 월

서울대학교 대학원

전기정보공학부

이 원 철

An effect of AC electrothermal flow on a carbon nanotube network based biosensor

AC electrothermal flow가 탄소나노튜브 네트워크 기반 바이오센서에 주는 효과

지도 교수 박 영 준

이 논문을 공학석사 학위논문으로 제출함

2017 년 2 월

서울대학교 대학원
전기정보공학부
이 원 철

이원철의 공학석사 학위논문을 인준함

2017 년 2 월

위 원 장 권 성 훈 (인)

부위원장 박 영 준 (인)

위 원 신 동 식 (인)

Abstract

The mechanism of various kinds of biosensors mainly depends on the chemical affinity between probe molecules immobilized on the sensor surface and the target molecules in the solution. The amount of target molecules can be inferred from the mechanical, optical, or electrical signal generated by probe-target binding events.

The binding process proceeds through two steps: the mass transport process and the surface reaction process. It is known that under the low target concentration condition, the binding rate is limited by the slow diffusive transport process.

To increase the probe-target binding rate, AC electrokinetics can be used to assist the transport process. Various methods such as AC electroosmosis, dielectrophoresis, AC electrothermal flow are suggested by other groups. Among them, AC electrothermal flow can have a significant effect in the conductive biological solution.

In this thesis, the effect of AC electrothermal flow on the biosensor performance is analyzed by both simulation and experiments. The carbon nanotube network based biosensor consists of concentric electrodes is used for identifying the effect of AC electrothermal flow. Simulation results indicate that AC electrothermal flow can assist the transport of target molecules toward the sensor surface and enhance the probe-

target binding rate. For experiments, a biomarker for acute myocardial infarction, cardiac troponin-I, is selected. Experimental results demonstrate AC electrothermal flow can boost the probe-target binding speed and significantly enhance the biosensor performance.

Keywords: Biosensor, Carbon nanotube, AC electrothermal flow, Cardiac troponin I (cTnI)

Student Number: 2015-20971

TABLE OF CONTENTS

List of Tables

List of Figures

Chapter 1. Introduction

1.1. Motivation

As the interest in monitoring one's health status and early diagnosis of incurable diseases increases, many researchers have tried to develop practical biomedical devices which can be used as convenient personalized diagnostic tools. Especially, it is argued that we could easily prevent and diagnose diseases by analyzing the amount of specific biomarker molecules in the clinical sample solutions, such as blood or serum.

For these reasons, during the past decades, many researchers have put an effort on developing biosensors which can detect specific molecules exist in biological solutions [1][2]. Many kinds of biosensor platforms, such as mechanical [3], optical [4], and electrochemical sensors [5], have been proposed. Basically, all these biosensors rely on the same mechanism, which is an affinity-based probe-target binding process as illustrated in Fig. 1.1. The capturing of target molecules by the probe molecules on the sensor surface generate mechanical, optical, and electrical

signals and by analyzing this signal, we could know the exact amount of molecules in the solution.

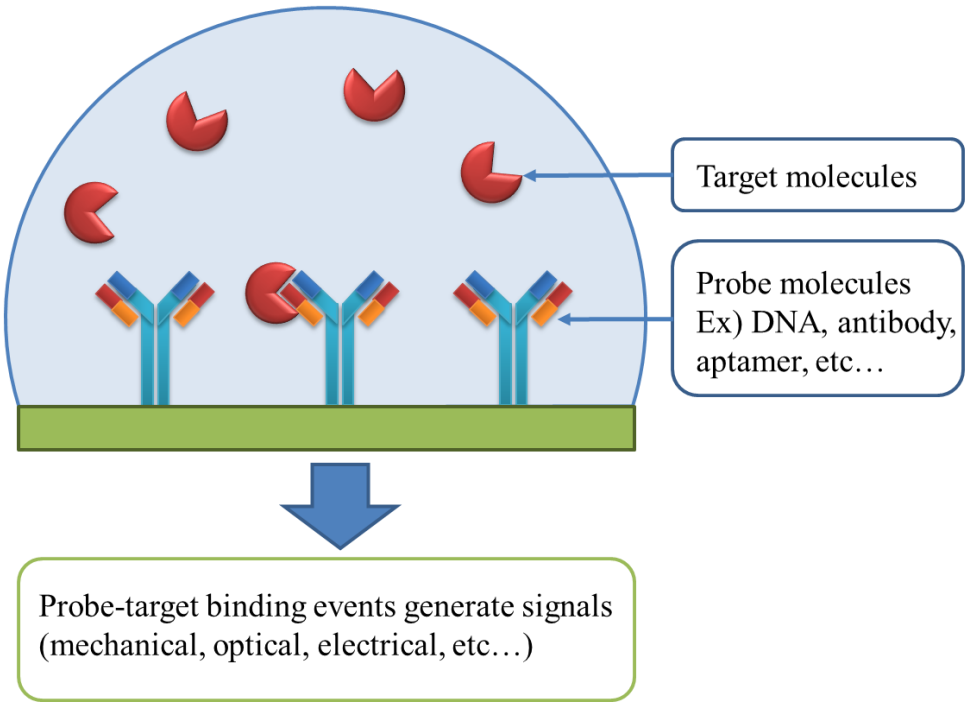

Fig. 1.1. Basic principles of affinity-based biosensors

The capturing process can be described by first-order Langmuir kinetics as:

$$\frac{\partial B}{\partial t} = k_{on} c_s (P - B) - k_{off} B, \quad (1)$$

where B is the surface concentration of the probe molecules bound by target molecules, P is the surface concentration of the probe molecules, c_s is the concentration of target molecules at the sensor surface, k_{on} is the association rate, and k_{off} is the dissociation rate.

However, there are some critical issues remained as a barrier against the realization of practical biosensors. For those biosensors to be used as fast point-of-care devices, the sensing speed should be much faster than nowadays products. And it is argued that it takes at least a few hours for sensing in case of solutions with a low concentration of the target molecule [6].

To analyze the fundamental reason of the slow sensing performance of biosensors, some researchers have analyzed the performance limit of nanobiosensors [7][8]. They asserted that the detection performance of an affinity-based biosensor is mainly limited by the transport process of biomolecules which mainly depends on the slow diffusion process.

If the clinical sample solution containing target molecules is applied to the sensor platform, the probe-target binding occurs at the sensor surface, according to Eq (1). As the target molecules at the sensor surface become depleted, the speed of the whole binding process is limited by the transport of the target molecules toward the sensor

surface. If there is no external force exerted on the target molecules, the transport of the target molecules occurs through diffusion process, as described by

$$\frac{\partial c}{\partial t} = D\nabla^2 c, \tag{2}$$

where c is the concentration of the target molecules and D is the diffusion coefficient of the target molecules.

From Eq (1) and Eq (2), the inverse relationship between the response time (t_s) and the minimum detectable concentration of a biosensor (c_0) can be inferred as $c_0 t_s^{M_D} \sim k_D$, where M_D and k_D are dimensionality-dependent constants [7]. The trade-off relationship between the sensing time and detectable concentration limit can be attributed to the 'diffusion limit'; in case of the low target concentration condition, their diffusive flux toward the sensor surface is very small and so that the probe-target binding occurs slowly. Thus, the response time of the biosensor increases. Therefore, to improve the detection time of a biosensor for better diagnostic performance, it is necessary to overcome the 'diffusion limit' of biosensors.

1.2. AC Electrokinetics for Enhancing Biosensor Performance

To deal with the fundamental limit, some researchers have suggested that by adopting alternating current (AC) electrokinetic methods, we can increase the transport rate of molecules in the solution. In recent years, AC electrokinetic forces have emerged as simple particle-manipulating methods that can be used in various microscale platforms [9][10][11]. The nonuniform electric field generated on the microelectrode structure by AC biasing can give rise to various types of phenomena such as AC electro-osmosis (ACEO), dielectrophoresis (DEP), and AC electrothermal flow (ACEF).

ACEO depends on the movement of diffuse charge in the electric double layer. Under AC bias condition, the ions in the diffuse layer move along the tangential component of the electric field and induce the flow as Fig. 1.2(a). Some researchers utilized ACEO for molecule concentration or particle trapping [12][13]. However, the effect of ACEO is not significant in highly conductive biological media because the thickness of the diffuse layer is inversely proportional to the conductivity of the

solution. As the diffuse layer is suppressed in the conductive biological solutions, the effect of ACEO also decreases. So it can be efficiently exploited in dilute solutions in which a thick electric double layer can be formed.

DEP is another electrokinetic method which is known to be effective for manipulating large particles (>1 μm) such as cells and bacteria. DEP depends on the interaction between the non-uniform electric field and the polarizability of the particle as expressed in Fig. 1.2(b). Many microfluidic platforms and sensors adopt this method to enhance their performance [14][15]. However, the problem of DEP is that it has a negligible effect on increasing the movement of small analytes (<100 nm) such as antigens, DNA, or peptides because the dielectrophoretic force is nearly proportional to the square of the particle radius [9][10].

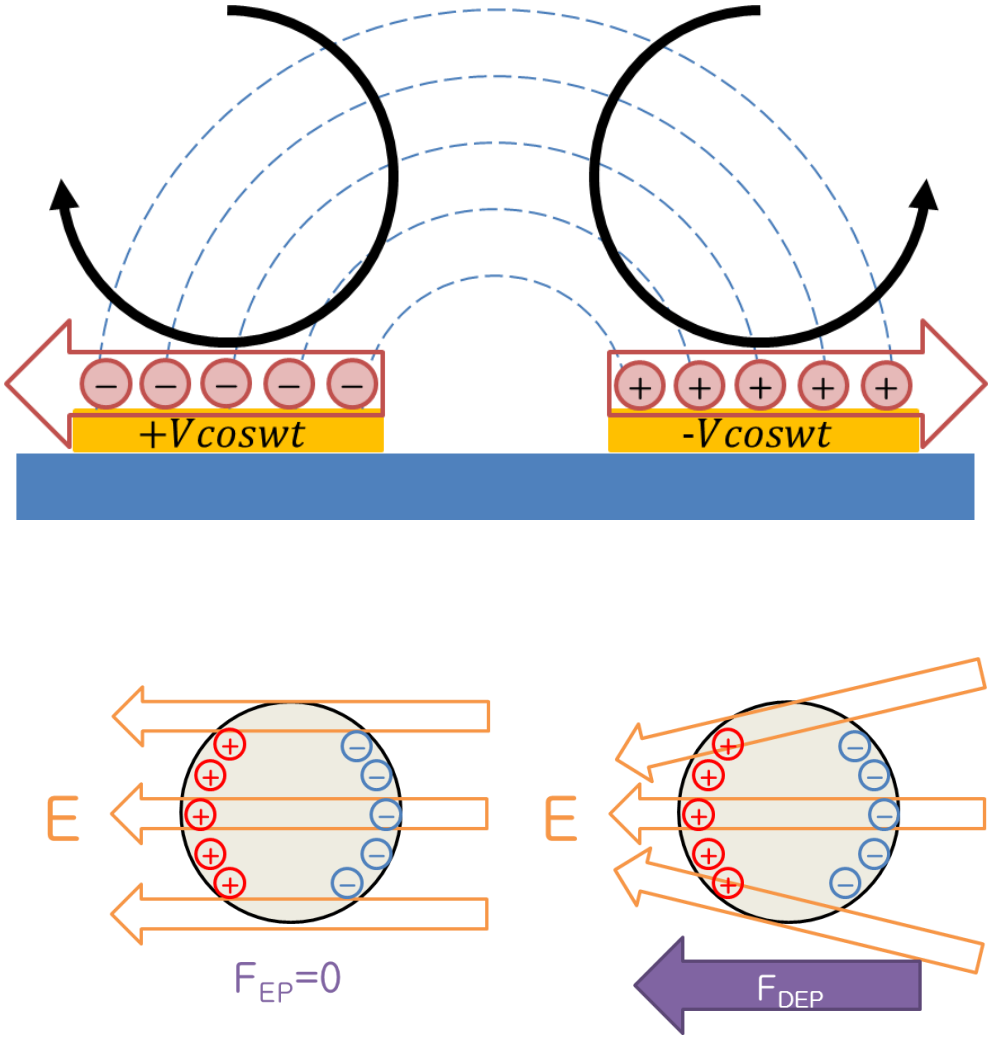

Fig. 1.2. Schematic illustration of the principle of (a) AC electroosmosis and (b) dielectrophoresis.

Compared with ACEO and DEP, ACEF is suitable for biomedical applications since it can effectively operate in highly conductive biological media (~ 1 S/m). ACEF results from the ionic conduction current that is driven by a nonuniform electric field. Then, an associated local Joule heating effect occurs and a locally increased temperature profile leads to gradients in the solution permittivity and conductivity. As a result of the combined effect of these gradients and the applied electric field, an electrokinetic force is exerted on the fluid so that various species of particles in the sample solution, even small molecules, can be stirred by the induced electrothermal flow.

1.3. Outline of Thesis

In this thesis, an effective affinity-based sensing strategy that can significantly enhance the sensing speed by combining the structural advantages of a carbon-nanotube-network (CNN)-based electrical biosensor platform and the microstirring effect of ACEF is demonstrated. For the investigation of the effect of ACEF, the carbon nanotube network based biosensor platform (C-chip) is selected. The C-chip

platform consists of two concentric electrodes; one is a small island electrode (IE) and the other is a large enclosing electrode (EE) as illustrated in Fig. 1.3 [16][17]. By applying AC bias between these two electrodes, a nonuniform electric field can be easily generated in the electrolyte and ACEF can be induced.

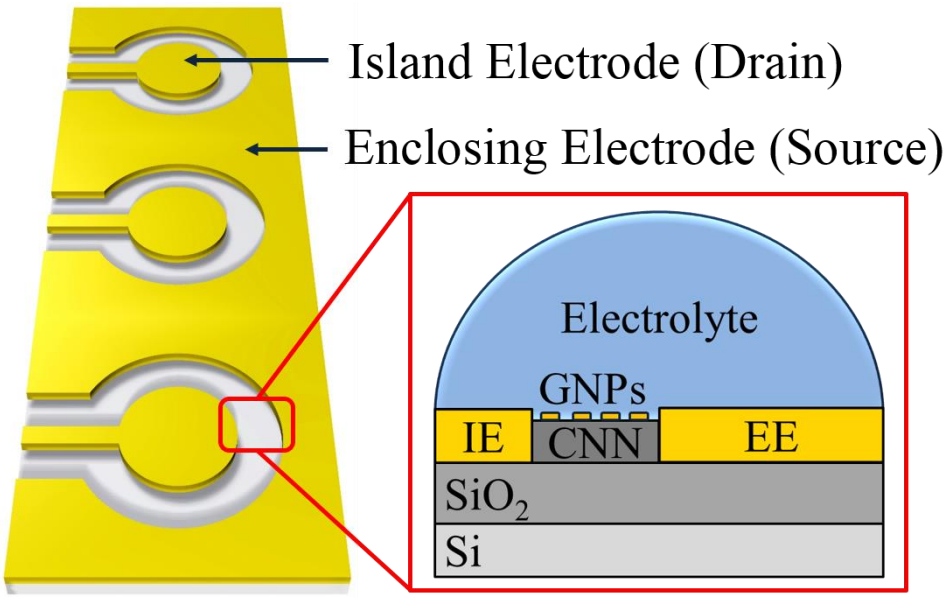

Fig. 1.3. Schematic representation of the biosensor platform with concentric electrodes.

The thermally induced flow contributes to the transport process with additional convective terms

$$\frac{\partial c}{\partial t} + \vec{v} \cdot \nabla c = D\nabla^2 c, \tag{3}$$

where $\vec{v}$ is the velocity of the fluid [9][10]. We used both simulations and experiments to verify that the ACEF induced using our biosensor platform can assist the transport of the target molecules toward the sensor surface so that the overall binding process can be accelerated, which leads to enhanced sensor performance.

This paper consists of five chapters from **Introduction** to **Conclusion**: In Chapter 1, a motivation and general overview of the AC electrokinetic methods are provided. The theoretical background and physical principles of AC electrokinetics are listed in Chapter 2. In Chapter 3, the numerical simulation of our platform implemented by COMSOL Multiphysics is provided. And the experimental verification of the simulations results by detecting cardiac troponin-I (cTnI), which is a specific cardiac biomarker for the diagnosis of acute myocardial infarction [18], can be found in Chapter 4. Finally, Chapter 5 is a conclusion part.

Chapter 2. Theoretical Background

2.1. Carbon Nanotube Network Based Biosensor Platform

Previously, a concentric shaped two-electrode platform which consists of small island electrode and large enclosing electrode was proposed [16][17]. The area of the enclosing electrode is about thousand times larger than island electrode. So if the sensor platform is immersed in the solution and the voltage is applied between the island electrode and the enclosing electrode, the potential of the solution is stabilized by the large area enclosing electrode. This is because the solution is capacitively coupled to the electrodes. At the electrode-electrolyte interface, an electric double layer develops as Fig. 2.1. The electric double layer consists of Stern layer that arises from the finite size of ions that adhere to the electrode and diffuse layer where the ion charge distribution follows Maxwell-Boltzmann statistics [19]. And they can be expressed as a series connection of capacitors.

On the concentric structure, a carbon nanotube network (CNN) is formed by the dip-coating method. The CNN region acts as a channel region of a field-effect

transistor. By the capacitive coupling between the electrode and the electrolyte, the potential of the electrolyte gate region is stabilized so that an additional gating electrode is not needed. This phenomenon is called as “self-gating effect” [16]. And the overall equivalent circuit diagram of the sensor platform can be expressed as Fig. 2.2.

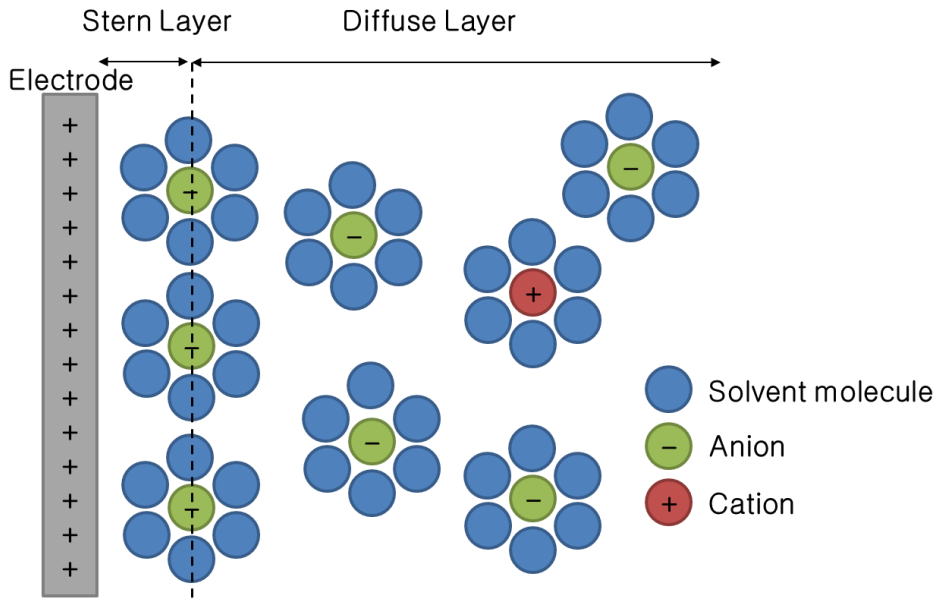

Fig. 2.1. Schematic illustration of electric double layer at the electrode-electrolyte interface.

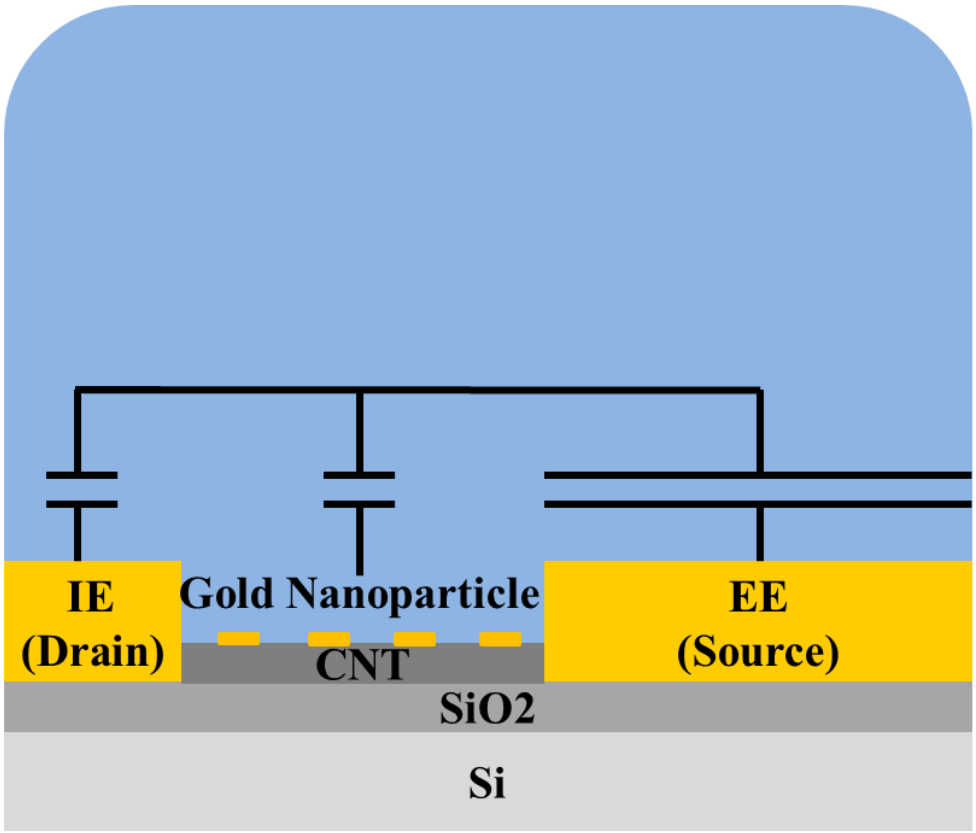

Fig. 2.2. Equivalent circuit diagram of the carbon nanotube network field effect transistor.

2.2. An Effect of AC Bias on DNA Hybridization Rates

Based on the C-chip platform, a DNA sensor is fabricated. Gold nanoparticles (GNPs) are immobilized on the platform and the probe DNA molecules which can be by target DNA molecules are assembled on the GNPs. So the binding reaction between probe and target DNA molecules leads to the change of current flow through the carbon nanotube network channel region [20]. From the current signal change, the amount of target DNA molecules in the solution can be deduced.

To enhance the probe-target hybridization rate, AC bias is applied to the sensor platform during the binding reaction occurs. By applying AC bias (Frequency: 1 kHz) to the drain (island electrode), the dynamic motion of the probe DNA immobilized on the channel region can be induced and this effect results in the change of the kinetic binding parameters as Fig. 2.3. The effect of AC bias on the enhancement of the surface reaction rate was identified by measuring the real-time current change during the probe-target binding time [21].

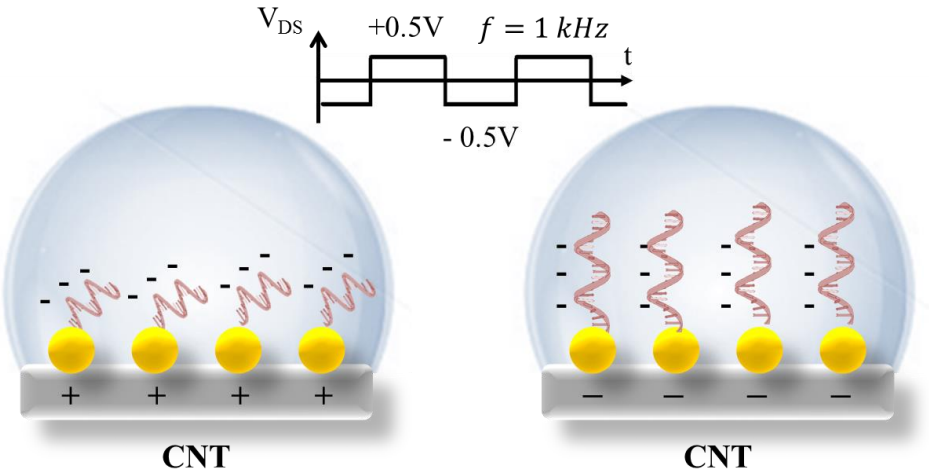

Fig. 2.3. Modulation of the hybridization rate of DNA molecules using AC biasing method.

2.3. Transient Measurement Method

The measurement in the conductive biological solutions (blood, serum, buffer solutions) suffer from the short Debye-length problem. In conductive solutions, the charge of the target molecules is screened by many counter ions in the solution so that

the field-effect of the biomolecules cannot have much effect on the current flows through the channel.

In order to overcome this problem, a simple electrical sensing method was suggested, which is called as a transient measurement method. If a step pulse is applied to the island electrode, the screening ions can be pushed back toward the bulk electrolyte so that the charge of the bound target molecules can reach the channel region as expressed in Fig. 2.4.

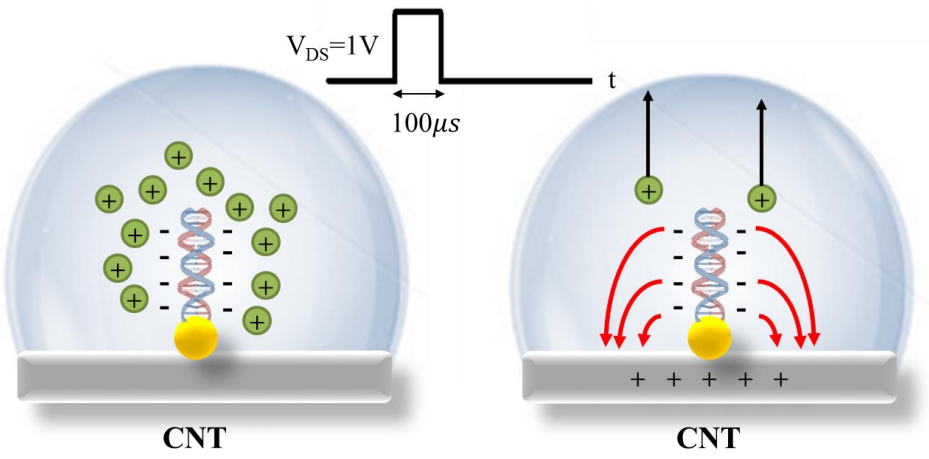

Fig. 2.4. Schematic illustration of transient measurement method.

Chapter 3. Simulation on the Effect of ACEF

3.1. Physical Principles of AC Electrothermal Flow

A theoretical analysis and equations describing principle of ACEF in a microscale system has been developed by other research groups and has been well-summarized in Ref [9][10]. Therefore, in this chapter only the core physical principles and equations describing the ACEF will be briefly reviewed. The following equations are used to simulate the two-dimensional cylindrical geometry which simplifies our sensor structure and to interpret the experimental data.

Since the most important factor to determine the probe-target binding process is the speed of the transport rate, an expression for $\vec{v}$ in Eq (3) must be obtained. To solve the problem, several assumptions should be made. First, it is assumed that the frequency of the AC signal is so high that we can neglect the polarization effect of the electrode. In other words, the effect of electric double layer will be neglected and the electrolyte region is considered as a simple resistive medium. Based on these

assumptions, the electric field $(\vec{E})$ and electric potential (V) in the electrolyte region can be obtained by solving Laplace equation as below:

$$\nabla^2 V = 0, \vec{E} = -\nabla V. \tag{4}$$

Then, the electric field induces the ionic conduction current and associated local Joule heating occurs. The local temperature (T) change induced by local Joule heating can be calculated by solving the energy balance equation

$$\rho_m c_p \vec{v} \cdot \nabla T + \rho_m c_p \frac{\partial T}{\partial t} = k\nabla^2 T + \sigma\left|\vec{E}\right|^2, \tag{5}$$

where ρ_m is the mass density of the fluid, c_p is the heat capacity of the fluid (at constant pressure), k is the thermal conductivity of the fluid, and σ is the electrical conductivity of the fluid.

And it is known that the electrical property of the solution depends on the temperature. The locally increased temperature profile induces the gradient of permittivity (ε) and conductivity (σ) of the solution as,

$$\nabla\varepsilon = (\partial\varepsilon/\partial T)\nabla T. \tag{6}$$

$$\nabla\sigma = (\partial\sigma/\partial T)\nabla T. \tag{7}$$

Because of these solution property changes, a space charge density (ρ) in the solution is also changed, which can be described by Gauss's law and the charge conservation equation,

$$\rho = \nabla \cdot \left(\varepsilon\vec{E}\right) = \nabla\varepsilon \cdot \vec{E} + \varepsilon\nabla \cdot \vec{E}, \tag{8}$$

$$\frac{\partial\rho}{\partial t} + \nabla \cdot \left(\sigma\vec{E}\right) = 0. \tag{9}$$

Then, the body force on the fluid can be expressed by the sum of Coulomb force and dielectric force,

$$\overrightarrow{F_E} = \rho\vec{E} + \frac{1}{2}\left|\vec{E}\right|^2\nabla\varepsilon \tag{10}$$

By solving the above equations, we can express the body force as expressed in Ref. 8

$$\overrightarrow{F_E} = -\frac{1}{2}\left[\left(\frac{\nabla\sigma}{\sigma} - \frac{\nabla\varepsilon}{\varepsilon}\right) \cdot \vec{E}\,\frac{\varepsilon\vec{E}}{1+(\omega\tau)^2} + \frac{1}{2}\left|\vec{E}\right|^2\nabla\varepsilon\right], \tag{11}$$

where $\tau = \varepsilon/\sigma$ is the charge relaxation time of the solution.

Finally, the thermally induced body force is exerted on the fluid and the induced flow velocity h can be solved by the Navier-Stokes equation

$$\rho_m \frac{\partial \vec{v}}{\partial t} + \rho_m \vec{v} \cdot \nabla \vec{v} = -\nabla p + \eta \nabla^2 \vec{v} + \vec{F_E}, \quad (12)$$

where p is the pressure, and η is the viscosity of the fluid.

The electrothermally induced fluid flow affects the transport of target molecules as described in Eq (3). Compared with a diffusion-limited case, in which target molecules are transported to the sensor surface only by the diffusive transport, as in Eq (2), the transport of target molecules to the sensor surface can be facilitated by the support of the convective transport. Since the convection process can modify the transport rate of target molecules, which is the limiting factor of the probe–target binding reaction, the probe-target binding rate can also be changed [22]. Therefore, by utilizing the effect of ACEF, we can enhance the performance of an affinity-based biosensor.

3.2. Simulation Methods

Based on these model equations, an effect of AC electrothermal flow on the performance of C-chip biosensor platform is investigated. To gain a clearer understanding of the physical principles and to determine the optimal experimental conditions, simulations were implemented. All simulations were performed using the finite element analysis software, COMSOL Multiphysics version 5.0 (COMSOL Ltd., Stockholm, Sweden). The simulation on the binding reaction of the target molecules (cTnI) with the probe molecules (Tro6 aptamer) is implemented for 30 min using a time-dependent solver.

The geometry used in the simulation is illustrated in Fig. 3.1. For the ACEF simulation, 2D cylindrical geometry is assumed. All the bottom boundaries are set as the binding region. A normal convergence test is implemented to determine that the simulation results are independent of the mesh used. All the geometric parameters are set to reflect the real size of the concentric device platform as illustrated in Fig. 7.

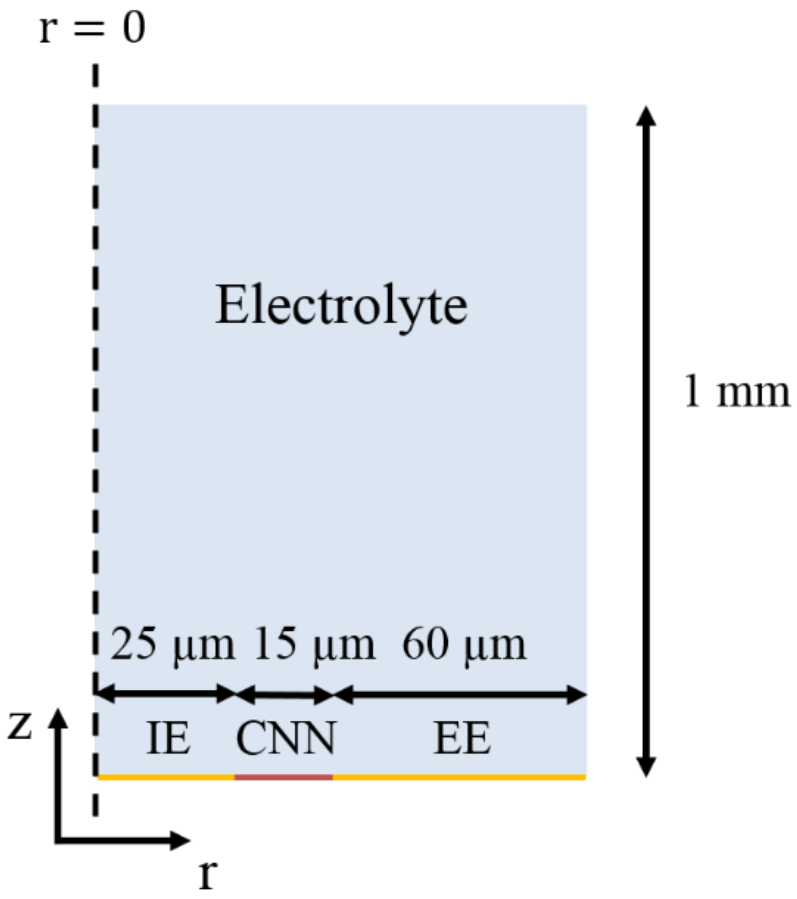

Fig. 3.1. Two-dimensional cylindrical geometry defined for the COMSOL simulation.

In case of electrical boundary conditions, the island electrode is set as constant potential $(V = V_{app})$ and the enclosing electrode is set as ground$(V = 0[V])$. Floating potential is assumed at the electrolyte boundaries toward bulk solution region and the

other boundaries are assumed as electrically insulated boundary [23]. And at all simulation region, the initial electrical condition is assumed as $V = 0$ [V].

Next, thermal boundary conditions are considered. First, the temperature at the surface of the two electrodes are set as $T = 293.15$ K. And an open boundary condition is assumed at the electrolyte boundaries so that the heat can flow out of the electrolyte by convection flux or flow into the electrolyte with a constant exterior temperature ($T_0 = 293.15$ K) [24]. And the thermal insulation condition is assumed on the other boundaries [23]. Initially uniform temperature condition ($T = 293.15$ K), is assumed in all simulation region.

Fluid boundary conditions are set as no slip condition at the sensor surface and zero pressure condition at the electrolyte boundaries [23][25]. The initial concentration of the target molecule (cTnI) is set as $c = 1$ nM for the simulations, and the electrolyte boundary is set as open boundary condition; the exterior concentration $c_0 = 1$ nM is assumed for the inflow and the convective flux condition is assumed for outflow [24]. And all bottom boundaries are set as a binding region.

The parameters used in the simulation are listed in the Table. I. The parameters of the solution region are chosen to reflect the characteristics of the real experimental condition.

Also, it is known that water shows temperature-dependent characteristics. For water, $(1/\sigma)(\partial\sigma/\partial T) = 0.02$ K^{-1} and $(1/\varepsilon)(\partial\varepsilon/\partial T) = -0.004$ K^{-1}[26]. And the reported value of the dissociation constant between Tro6 aptamer molecules and cTnI molecules ($K_{\mathrm{d}} = 317$ pM) is considered in the simulation [27]. The association rate constant (k_{on}) and the dissociation constant (k_{off}) are assumed to satisfy the following relation, $k_{\mathrm{off}}/k_{\mathrm{on}} = K_{\mathrm{d}} = 317$ pM . The diffusion constant of cTnI molecules ($D = 0.1 \times 10^{-9}$ m^2/s) is obtained from Ref [28].

Table 3.1. Simulation Parameters

Parameters	Values	Description
ε_r	78.5	Relative permittivity of the solution
σ	1 S/m	Electrical conductivity of the solution
ρ_m	10^3 kg/m^3	Solution mass density
c_p	4484 J kg^{-1} K^{-1}	Heat capacity of the solution
k	0.598 W m^{-1}K^{-1}	Thermal conductivity of the solution
η	$10^{-3} Pa \cdot s$	Viscosity of the solution
D	0.1×10^{-9} m^2/s	Diffusion constant of the target molecule
k_{on}	10^7 L mol^{-1} s^{-1}	Association rate constant
k_{off}	3.17×10^7 s^{-1}	Dissociation rate constant
P	10^{13} cm^{-2}	Surface density of the probe molecule
V_{app}	0, 1, 3, 5 V	Applied bias voltage

3.3. Simulation Results

To identify the effect of AC electrothermal flow, the concentration of the target molecules near the sensor surface is analyzed at various bias conditions. Fig. 3.2 shows the concentration of the target molecules at various bias conditions after 60 seconds of binding time. From the simulation results, two noticeable phenomena that are related with the AC electrothermal effect are identified.

First, as the bias amplitude increases, the degree of the depletion of the target molecules near the sensor surface significantly decreases. This result indicates that the transport of target molecules from the electrolyte to the sensor surface is enhanced and thus suppresses the depletion of the target molecules at the sensor surface. Especially, the degree of suppression of the depletion zone is at a maximum exactly above the CNN region which acts as sensing region.

To identify the exact physical principle of the change, the flow velocity field is analyzed at 5V AC bias condition in Fig. 3.2(e). The velocity field plot shows that a fast vortex, of which maximum speed is about 1.5×10^{-3} m/s, is formed right above the sensor surface. This electrothermally induced vortex contributes to the transport

of target molecules by the convective process as Eq (3). Therefore the target molecules are continuously transported to the CNN region by the microstirring effect of the induced vortex. The location of the induced vortex indicates that our sensor platform with concentric electrodes has an extremely suitable geometry to utilize the effect of ACEF.

Second, the probe-target binding rate is significantly enhanced due to the application of ACEF. To compare the binding rate under the both AC biased and unbiased cases, the dimensionless bound probe molecule (B/B_{eq}) is investigated, where B_{eq} represents the surface concentration of the bound probe molecules under the equilibrium condition, in Fig. 3.3(a) and 3.3(b) for the unbiased conditions and 5V AC biased conditions, respectively. For the various concentration of the target molecules, the probe-target binding process proceeds nearly 10 times faster under AC biased condition.

These two evident phenomena indicate that the utilization of the effect of ACEF can be extremely useful for enhancing the probe-target binding rate, thereby shortening the detection time of biosensors.

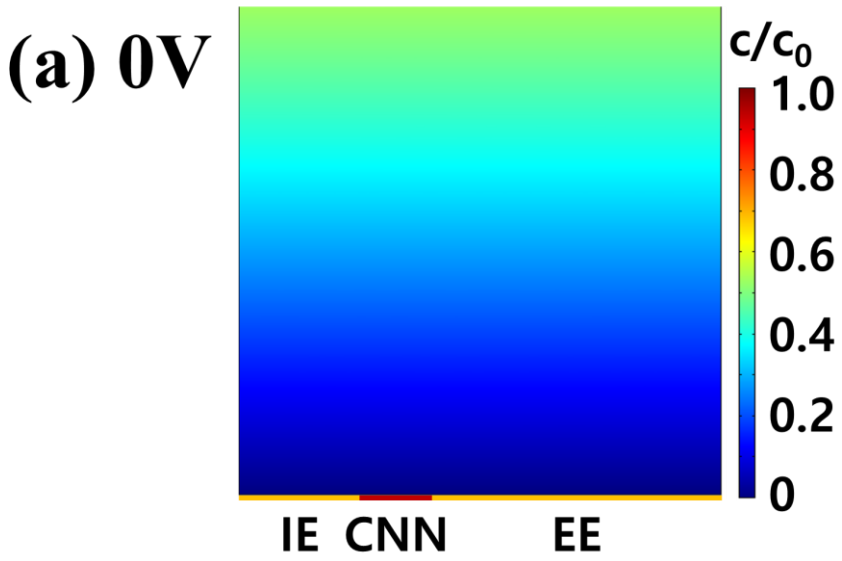
(a) 0V
c/c0
1.0
0.8
0.6
0.4
0.2
0
IE
CNN
EE

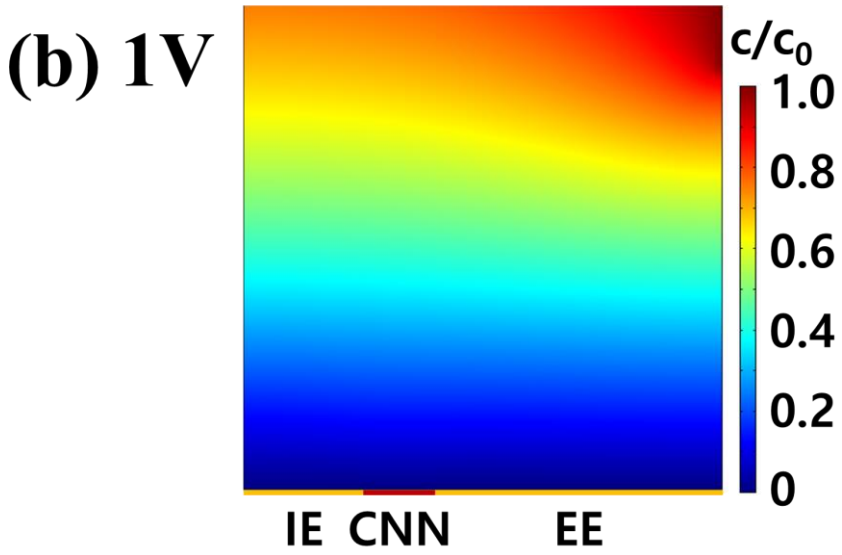
(b) 1V
c/c0
1.0
0.8
0.6
0.4
0.2
0
IE
CNN
EE

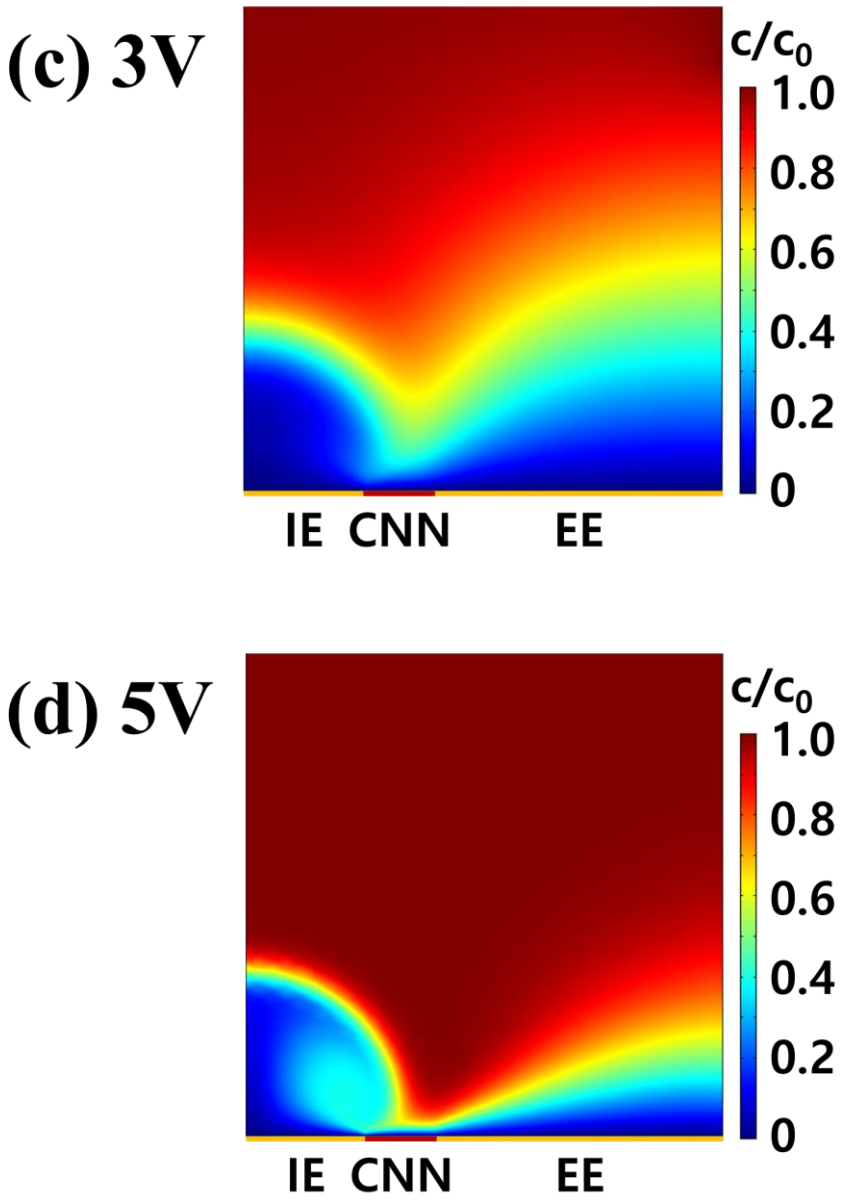

Fig. 3.2. Concentration field calculated under various AC amplitudes (V_{app}), (a) V_{app}=0V, (b) V_{app}=1V, (c) V_{app}=3V, and (d) V_{app}=5V

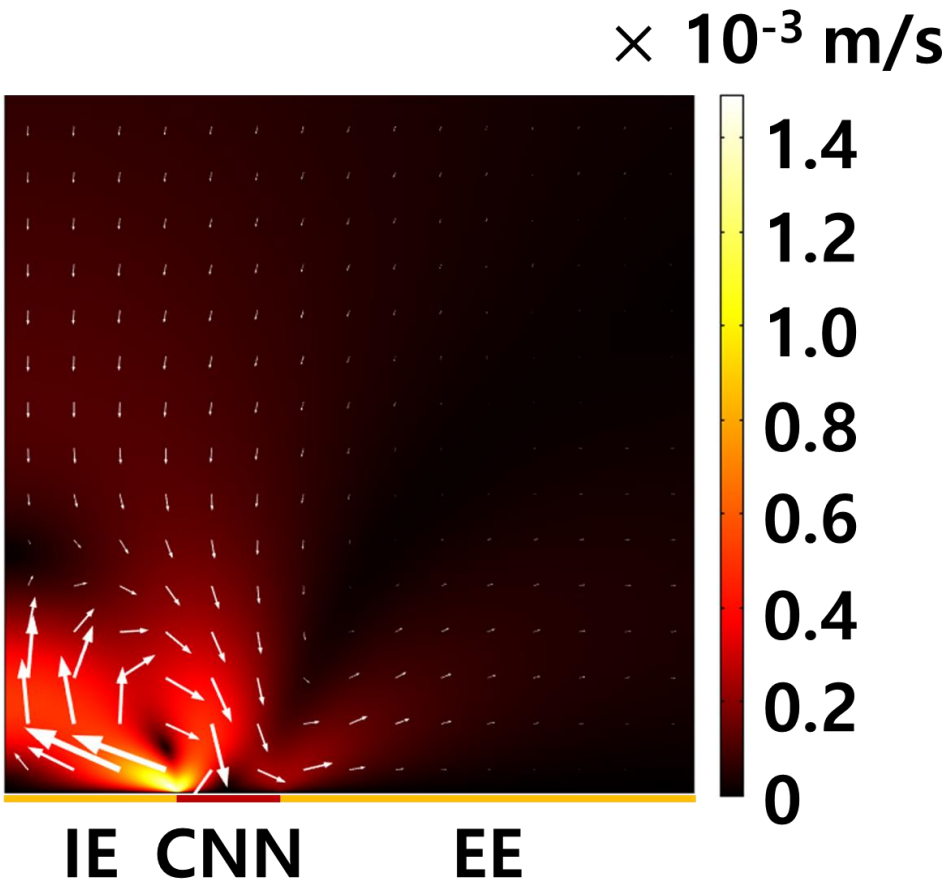

Fig. 3.3. Simulated velocity field for V_{app}=5V.

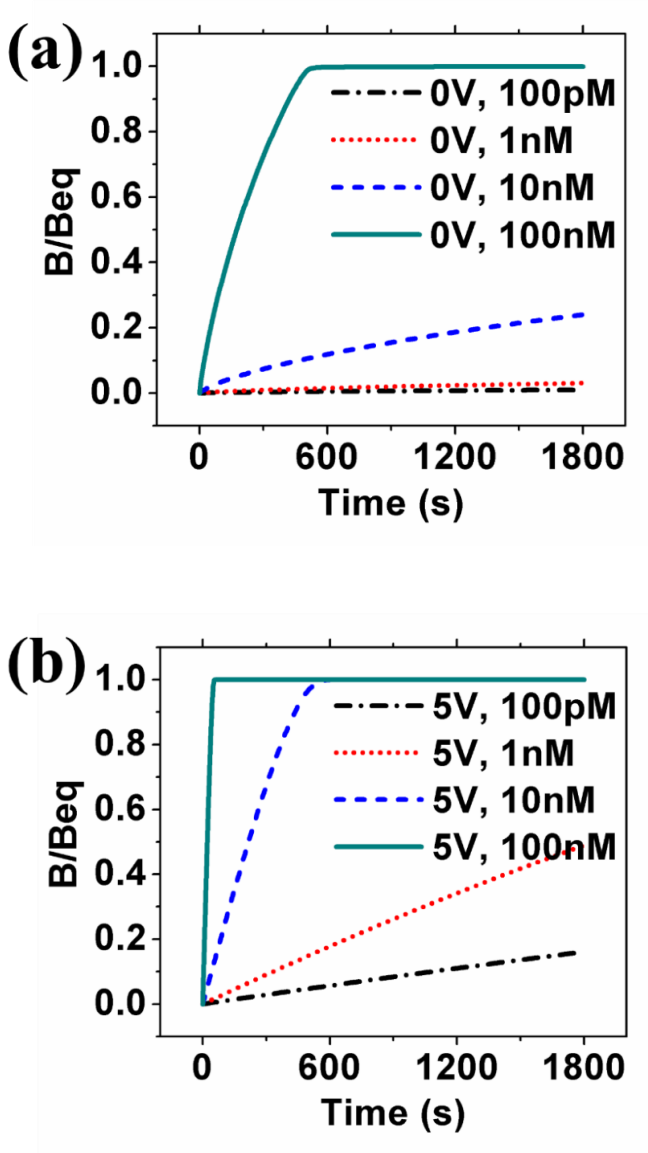

Fig. 3.4. Dimensionless bound probe molecule B/B_{eq} as a function of time under (a) unbiased conditions and (b) 5V AC bias.

Chapter 4. Experimental Results and Discussion

4.1. Preparation of the Biosensor Platform

Based on the simulation results, experiments are implemented for the sensing of cTnI using the previously developed sensor platform as depicted in Fig. 4.1(a). On the sensor platform consists of concentric electrodes and carbon nanotube network channel region, gold nanoparticles (GNPs) were deposited by a thermal evaporation process, as reported previously [21]. The GNPs act as immobilizing sites of probe molecules. The GNPs decorated on the CNN were evaluated by field emission scanning electron microscopy (FE-SEM) as illustrated in Fig. 4.1(a). The CNN (black lines in the figure) and the GNPs (white dots in the figure) can be clearly identified from the SEM images.

After fabrication of the CNN-GNP-FET device, probe molecules are immobilized on the sensor platform. The sensor structure was incubated in a phosphate-buffered saline (PBS) solution containing a 5'-thiol modified Tro6 aptamer (10 μM) at room temperature for 1 h. Tro6 is a DNA aptamer that has a high chemical affinity and

specificity to cTnI. During the 1 h of incubation process, Tro 6 aptamers are self-assembled on the GNPs by forming gold-thiol chemical bonds.

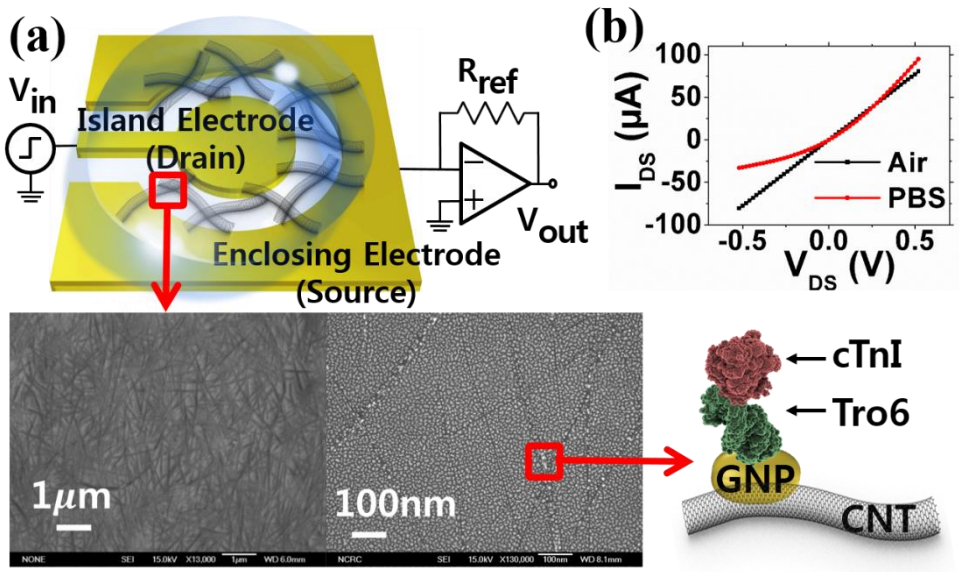

Fig. 4.1. (a) Schematic representation of the carbon nanotube network based biosensor platform for detecting cardiac troponin-I and (b) I-V characteristics of the sensor.

To monitor whether Tro6 aptamer molecules are well anchored on the GNPS, the real-time current flow through the CNN was monitored during the immobilization

process (Fig. 4.2). Constant voltage (0.1 V) was applied to the drain (island electrode) and the current was measured. An inverting operational amplifier circuit was used to convert the output current to voltage signals as expressed in Fig. 4.1. To compare with the normal PBS solution which does not contain a Tro6 aptamer, the normalized current is analyzed by dividing the real-time current by the initial current. As we can see from Fig. 4.2, the current change in the Tro6 aptamer solution was more significant compared with the normal PBS solution. This difference can be attributed to the modulation of the work function of GNPs induced by the formation of gold-thiol chemical bonds [20].

After Tro6 aptamer immobilization process, the sensor platform was washed with deionized water for 30 s to remove Tro6 aptamers which are nonspecifically bound to the sensor platform.

Also, the electrical characteristics of the channel is an important factor in a FET-based biosensor. It is reported that a carbon nanotube network tends to show p-type characteristics [16][17] or ambipolar characteristics [29][30] depends on fabrication processes or environmental conditions. And illustrated in Fig. 4.1(b), the CNN used in our experiments showed p-type semiconductor behavior.

For cTnI sensing experiments, solutions with different concentrations of cTnI (from 100 pM to 100 nM) were applied to the aptamer-modified CNN-GNP-FET. All the chemicals and solvents used in the experiments were reagent grade and used without further purification. The Tro6 aptamer was purchased from Bioneer Inc. (Korea). PBS solution (NaCl: 150 mM, pH 7.6) was purchased from Sigma-Aldrich Inc. (Korea).

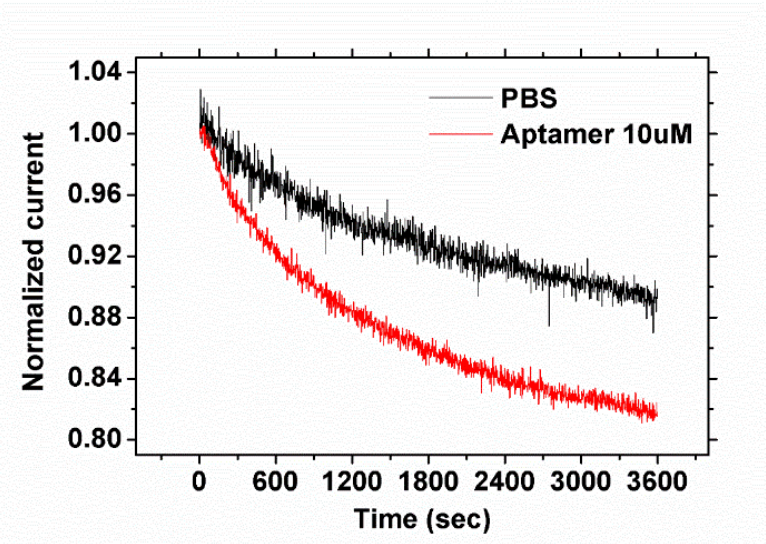

Fig. 4.2. Real-time monitoring of current flow during the Tro6 aptamer immobilization process.

4.2. Experimental Conditions

For cTnI sensing, two distinctive electrical techniques were applied to the sensor platform. First, to enhance the probe-target binding process, we applied AC bias (5V amplitude, 1 MHz frequency) for 30 min (for probe-target binding) to invoke the ACEF. To maximize the effect of ACEF, we considered the frequency-dependence of AC electrothermal effect.

In case of low frequencies, the polarization of the electrode occurs and leads to the decrease of the electric field in the bulk electrolyte. In case of the C-chip biosensor platform, the RC time in the solution is approximately a few microseconds [21]. Since the electrothermal effect is very sensitive to the strength of the electric field as described in Eq (10), we have to prevent the polarization to maximize the effect of ACEF.

Meanwhile, we can get a sight from the Eq (10) that too high-frequency conditions can weaken the electrothermal effect because the frequency and the fluid body force are inversely related with each other. Also, other groups reported experimental results that the velocity of the fluid becomes weaken at too high-frequency conditions [31].

Next, the amplitude of the AC bias is considered. As mentioned in Chapter 3, a higher electric field leads to much stronger fluid body force (Eq (10)). Also, it is verified by the simulation results that the higher amplitude bias led to the more significant effect of ACEF. But in the actual experimental condition, when a high voltage bias is applied to the electrode, severe electrolysis can occur [32]. However, electrolysis can be avoided by the selection of a 1 MHz frequency because only a small fraction of the applied potential drops across the thin electric double layer [10][11]. However, even the degradation of the sensor platform and water electrolysis were observed at bias amplitudes above 5V; therefore, 5V bias is selected as the bias amplitude for the experiments.

After the mixing step, a transient measurement was performed for cTnI sensing, which has previously been reported [21]. The step pulse (1 V amplitude, 100 μs duty) generated by the function generator was applied to the CNN and the current was converted to voltage signals through an inverting operational amplifier circuit. The merit of the transient measurement is that it can relieve the charge-screening effect in very conductive solutions, where the Debye length is very short (~1 nm). By applying a step pulse to the island electrode, counter ions surrounding the charged target

molecules bound to the channel region were swept away, so that the field effect of these charged target molecules on the CNN channel region can be significantly amplified. Because the output of the transient measurement includes both the capacitive current flows through the electrolyte and the channel current flows through the CNN channel region, as illustrated in Fig. 4.3, the channel current is calculated by subtracting the capacitive current from the total current. Sensitivity is defined as the ratio of the difference in channel current before and after probe–target hybridization to the channel current before probe–target hybridization.

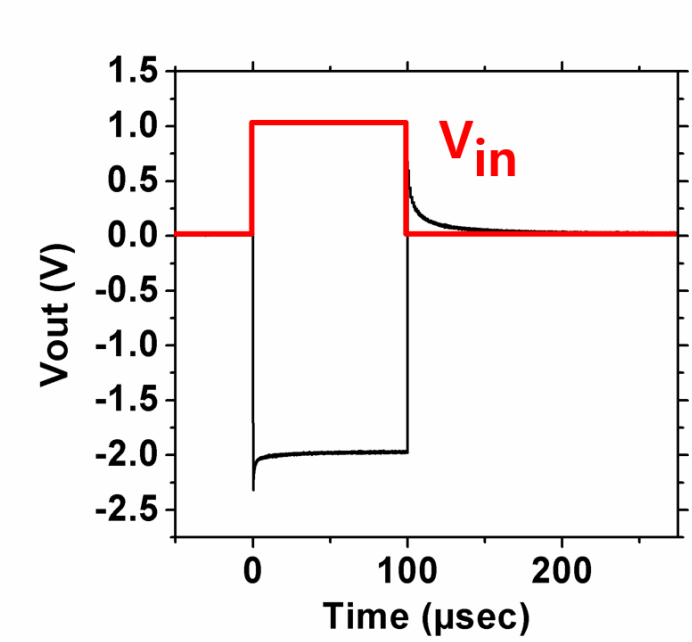

Fig. 4.3. Applied input bias and output versus time in transient measurements.

4.3. An Effect of ACEF on the Sensitivity of the Biosensor

Transient measurement results after 30min of AC bias and no bias are compared in Fig. 4.4(a) and 4.4(b). In the AC bias experiments, a clear response was obtained at cTnI concentrations of 100 pM to 100 nM. cTnI molecule has a positive charge in the PBS solution (pH 7.4) since the isoelectric point of cTnI is 9.87. Therefore, the cTnI molecules captured by the Tro6 aptamer molecules were expected to show a positive-gating effect on the carbon nanotubes, which directly led to the decrease of the current through the p-type CNN region.

Meanwhile, it has also been reported that the doping effect from the captured target molecules is the main sensing mechanism of carbon nanotube biosensors [33][34]. Therefore, both the electrostatic gating effect and molecular doping effect should be considered as sensing mechanisms. However, in the perspective of the doping effect, positively charged cTnI would cause hole-doping effects and the sensitivity to decrease, which is contrary to the experimental data. Therefore, the signal change obtained from the experiments can be attributed to the dominant influence of the electrostatic gating effect of the captured cTnI molecules.

Without AC bias, an inferior sensing performance was observed compared with the clear sensing signal obtained in the experiments under AC bias. cTnI molecules were only detectable at concentrations of 100 nM and the sensor failed to detect lower concentrations of cTnI. These results demonstrate that ACEF is very effective at increasing the probe–target binding rate, and consequently, improving the detection limit of the biosensor by approximately 1–2 orders of magnitude.

4.4. Selectivity of the Biosensor

The selectivity of the sensor platform, which is another important performance factor for a biosensor, is also investigated. For control experiments, bovine serum albumin (BSA), thrombin, and ErbB2 are selected. Although the high concentrations of these non-target molecules (100 nM) were tested, the observed sensitivity was only approximately 5% as expressed in Fig. 4.4(c). This value was much smaller than the sensitivity value obtained from the experiment with the same concentration of cTnI. These results indicate that the sensor can selectively detect the target molecule cTnI among various non-target molecules.

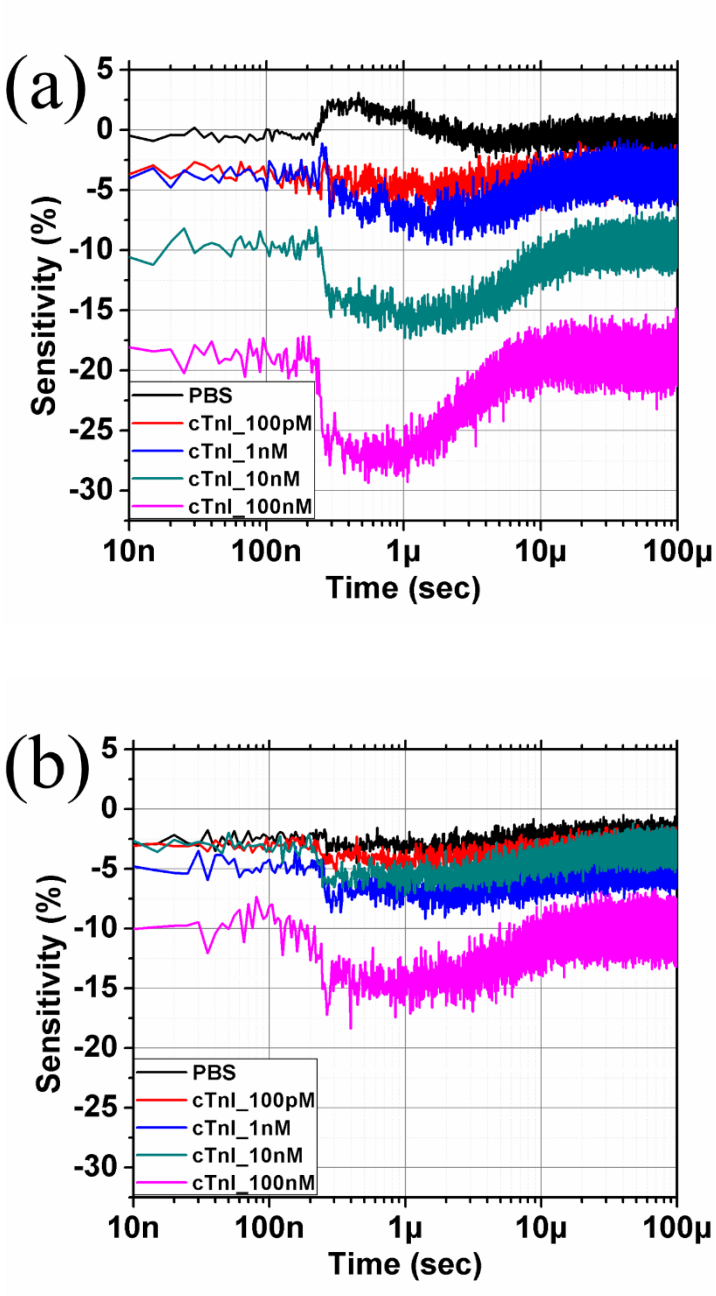

Fig. 4.4. Transient measurement after 30min under (a) AC biased condition and (b) unbiased condition

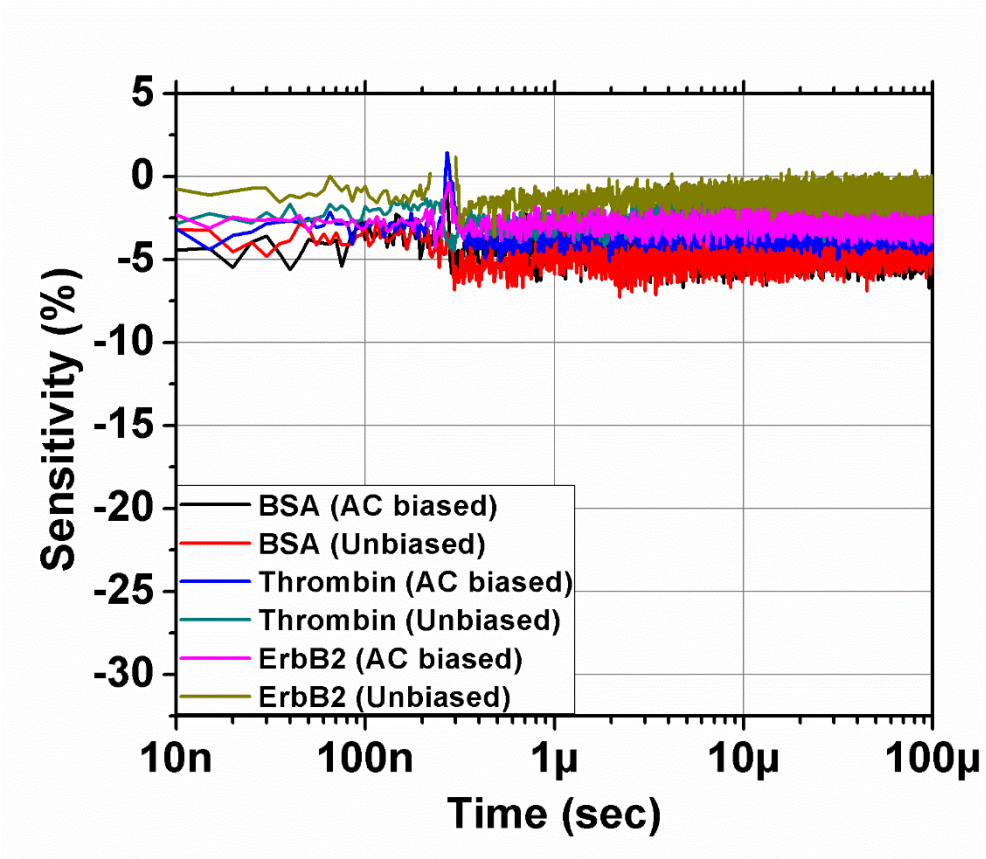

Fig. 4.5. Selectivity of the biosensor.

4.5. An Effect of ACEF on the Settling Time of the Biosensor

In addition, the settling time of a sensor, which is considered as one of the important indicators of the biosensor performance, is analyzed. Transient measurements were performed every 10 min for 90 min under both AC bias and unbiased conditions in 100 nM cTnI solution as Fig. 4.4(d). The plotted value indicates the average value of the 10 measurement points (100 ns) around 1 μs where a maximum sensitivity value is measured. Under the unbiased condition, the sensor signal of the C-chip biosensor platform did not reach the saturation point even after 90 min of measurement in 100 nM cTnI solution. This result coincides with the reported trend that it can take more than an hour for a sensor signal to reach a steady state [6]. However, under the AC biased condition, the sensitivity changed faster than the unbiased case and after 90min of the measurement, the signal almost reached the saturation point. This experimental result demonstrates that the settling time of the biosensor can be reduced by utilizing ACEF.

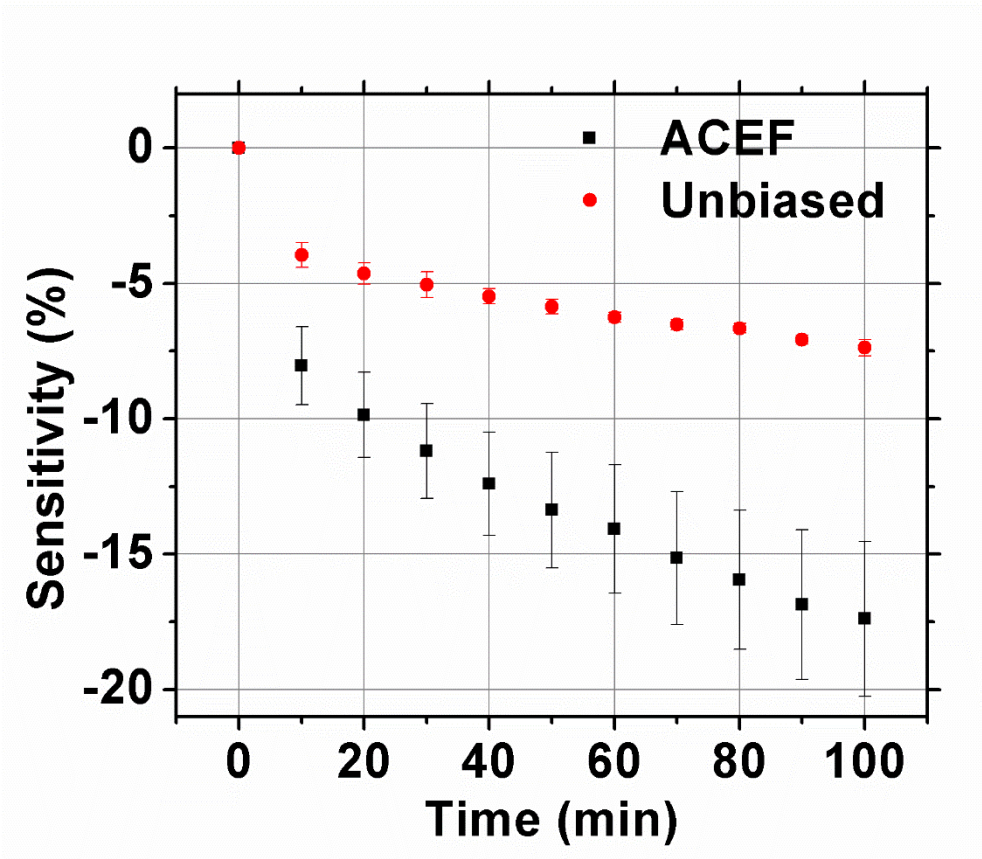

Fig. 4.6. An effect of ACEF on the settling time of the biosensor signal

Chapter 5. Conclusion

In this thesis, an effective electrical sensing scheme using the ACEF effect on a concentric CNN-based platform was demonstrated. The effect of ACEF on the performance of the biosensor was examined by performing both simulation and experimental studies on the sensing of cTnI. The simulation results indicate that the concentric electrode structure is advantageous for invoking ACEF and thus enhance the transport of target molecules toward the sensor surface. The experimental results on the cTnI sensing show that the detection performance is extremely enhanced under AC bias compared with under no bias condition. These results demonstrate that adopting the effect of ACEF at the biosensor can be very effective at improving the detection performance of various sensor platforms.

Bibliography

[1] P. B. Luppa, L. J. Sokoll, and D. W. Chan, "Immunosensors—principles and applications to clinical chemistry," *Clin. Chim. Acta*, vol. 314, no. 1–2, pp. 1–26, 2001.

[2] M. U. Ahmed, I. Saaem, P. C. Wu, and A. S. Brown, "Personalized diagnostics and biosensors: a review of the biology and technology needed for personalized medicine," *Crit. Rev. Biotechnol.*, vol. 34, no. 2, pp. 180–196, 2014.

[3] J. L. Arlett, E. B. Myers, and M. L. Roukes, "Comparative advantages of mechanical biosensors," *Nat. Nanotechnol.*, vol. 6, no. 4, pp. 203–215, 2011.

[4] X. Fan, I. M. White, S. I. Shopova, H. Zhu, J. D. Suter, and Y. Sun, "Sensitive optical biosensors for unlabeled targets: A review," *Anal. Chim. Acta*, vol. 620, no. 1–2, pp. 8–26, 2008.

[5] X. Luo and J. J. Davis, "Electrical biosensors and the label free detection of protein disease biomarkers," *Chem. Soc. Rev.*, vol. 42, no. 13, pp. 5944–62, 2013.

[6] G. Xu, J. Abbott, and D. Ham, "Optimization of CMOS-ISFET-Based Biomolecular Sensing: Analysis and Demonstration in DNA Detection," *IEEE Trans. Electron Devices*, vol. 63, no. 8, pp. 3249–3256, 2016.

[7] P. R. Nair and M. A. Alam, "Performance limits of nanobiosensors," *Appl. Phys. Lett.*, vol. 88, no. 23, 2006.

[8] P. E. Sheehan and L. J. Whitman, "Detection Limits for Nanoscale Biosensors," *Nano Lett.*, vol. 5, no. 4, pp. 803–807, Apr. 2005.

[9] A. Ramos, H. Morgan, N. G. Green, and a Castellanos, "AC electrokinetics: a review of forces in microelectrode structures," *J. Phys. D. Appl. Phys.*, vol. 31, no. 18, pp. 2338–2353, 1999.

[10] A. Castellanos, A. Ramos, A. González, N. G. Green, and H. Morgan, "Electrohydrodynamics and dielectrophoresis in microsystems: scaling laws," *J. Phys. D. Appl. Phys.*, vol. 36, no. 20, pp. 2584–2597, Oct. 2003.

[11] P. K. Wong, T.-H. Wang, J. H. Deval, and C.-M. Ho, "Electrokinetics in Micro Devices for Biotechnology Applications," *IEEE/ASME Trans. Mechatronics*, vol. 9, no. 2, pp. 366–376, Jun. 2004.

[12] M. R. Bown and C. D. Meinhart, "AC electroosmotic flow in a DNA concentrator," *Microfluid. Nanofluidics*, vol. 2, no. 6, pp. 513–523, 2006.

[13] J. Wu, Y. Ben, D. Battigelli, and H. C. Chang, "Long-range AC electroosmotic trapping and detection of bioparticles," *Ind. Eng. Chem. Res.*, vol. 44, no. 8, pp. 2815–2822, 2005.

[14] M. Javanmard, S. Emaminejad, C. Gupta, J. Provine, R. W. Davis, and R. T. Howe, "Depletion of cells and abundant proteins from biological samples byenhanced dielectrophoresis," *Sensors Actuators, B Chem.*, vol. 193, pp. 918–924, 2014.

[15] X. Hu, P. H. Bessette, J. Qian, C. D. Meinhart, P. S. Daugherty, and H. T. Soh, "Marker-specific sorting of rare cells using dielectrophoresis," *Proc. Natl. Acad. Sci.*, vol. 102, no. 44, pp. 15757–15761, 2005.

[16] D. W. Kim, G. S. Choe, S. M. Seo, J. H. Cheon, H. Kim, J. W. Ko, I. Y. Chung and Y. J. Park, "Self-gating effects in carbon nanotube network based liquid gate field effect transistors," *Appl. Phys. Lett.*, vol. 93, no. 24, 2008.

[17] J. H. Cheon, J. Lim, S. M. Seo, J. M. Woo, S. H. Kim, Y. Kwon, J. W. Ko, T. J. Kang, Y. H. Kim and Y. J. Park, "Electrical characteristics of the concentric-shape carbon nanotube network device in pH buffer solution," *IEEE Trans. Electron Devices*, vol. 57, no. 10, pp. 2684–2689, 2010.

[18] M. C. Fishbein, T. Wang, M. Matijasevic, L. Hong, and F. S. Apple, "Myocardial tissue troponins T and I: An immunohistochemical study in experimental models of myocardial ischemia," *Cardiovasc. Pathol.*, vol. 12, no. 2, pp. 65–71, 2003.

[19] A. J. Bard and L. R. Faulkner, *Electrochemical Methods: Fundamentals and Applications*, 2nd ed. (Wiley, 2004)

[20] J.W. Ko, J.M. Woo, A. Jinhong, J.H. Cheon, J.H. Lim, S.H. Kim, H. Chun, E. Kim, and Y.J. Park, "Multi-order dynamic range DNA sensor using a gold decorated SWCNT random network," *ACS Nano*, vol. 5, no. 6, pp. 4365–4372, 2011.

[21] J.-M. Woo, S. H. Kim, H. Chun, S. J. Kim, J. Ahn, and Y. J. Park, "Modulation of molecular hybridization and charge screening in a carbon nanotube network

channel using the electrical pulse method," *Lab Chip*, vol. 13, no. 18, pp. 3755–63, 2013.

[22] T. M. Squires, R. J. Messinger, and S. R. Manalis, "Making it stick: convection, reaction and diffusion in surface-based biosensors," *Nat. Biotechnol.*, vol. 26, no. 4, pp. 417–426, 2008.

[23] N. G. Green, A. Ramos, A. González, A. Castellanos, and H. Morgan, "Electrothermally induced fluid flow on microelectrodes," *J. Electrostat.*, vol. 53, no. 2, pp. 71–87, 2001.

[24] COMSOL Multiphysics, User's Guide, version 5.0 (2014).

[25] C. K. Yang, J. S. Chang, S. D. Chao, and K. C. Wu, "Two dimensional simulation on immunoassay for a biosensor with applying electrothermal effect," *Appl. Phys. Lett.*, vol. 91, no. 11, 2007.

[26] D. R. Lide, *CRC handbook of Chemistry and Physics*, 81st ed. (CRC, New York, 2000).

[27] H. Jo, H. Gu, W. Jeon, H. Youn, J. Her, S.K. Kim, J. Lee, J.H. Shin, and C. Ban, "Electrochemical Aptasensor of Cardiac Troponin i for the Early Diagnosis of Acute Myocardial Infarction," *Anal. Chem.*, vol. 87, no. 19, pp. 9869–9875, 2015.

[28] T. Jacroux, D. Bottenus, B. Rieck, C. F. Ivory, and W. Dong, "Cationic isotachophoresis separation of the biomarker cardiac troponin I from a high-

abundance contaminant, serum albumin," *Electrophoresis*, vol. 35, no. 14, pp. 2029–2038, Jul. 2014.

[29] G. Xu, F. Liu, S. Han, K. Ryu, A. Badmaev, B. Lei, C. Zhou, and K. L. Wang, "Low-frequency noise in top-gated ambipolar carbon nanotube field effect transistors," *Appl. Phys. Lett.*, vol. 92, no. 22, pp. 2006–2009, 2008.

[30] V. Derenskyi, W. Gomulya, J. M. S. Rios, M. Fritsch, N. Frohlich, S. Jung, S. Allard, S. Z. Bisri, P. Gordiichuk, A. Herrmann, U. Scherf, and M. A. Loi, "Carbon Nanotube Network Ambipolar Field-Effect Transistors with 108 On/Off Ratio," *Adv. Mater.*, vol. 26, no. 34, pp. 5969–5975, 2014.

[31] M. L. Y. Sin, V. Gau, J. C. Liao, and P. K. Wong, "Electrothermal fluid manipulation of high-conductivity samples for laboratory automation applications," *JALA - J. Assoc. Lab. Autom.*, vol. 15, no. 6, pp. 426–432, 2010.

[32] C.H. Hamann, A. Hamnett, and W. Vielstich, *Electrochemistry* (Wiley-VCH: Weinheim, 1997)

[33] A. Star, E. Tu, J. Niemann, J.-C. P. Gabriel, C. S. Joiner, and C. Valcke, "Label-free detection of DNA hybridization using carbon nanotube network field-effect transistors," *Proc. Natl. Acad. Sci.*, vol. 103, no. 4, pp. 921–926, 2006.

[34] G. Xu, J. Abbott, L. Qin, K. Y. M. Yeung, Y. Song, H. Yoon, J. Kong, and D. Ham, "Electrophoretic and field-effect graphene for all-electrical DNA array technology.," *Nat. Commun.*, vol. 5, p. 4866, 2014.

초록

다양한 종류의 바이오센서의 동작 원리는 기본적으로 용액 내에 존재하는 타겟 분자와 센서 표면의 프로브 분자 간의 화학적 결합에 의존한다. 이러한 화학적 결합에 의해 기계적, 광학적, 전기적 신호가 생성되고 이를 통해 수용액 내에 존재하는 타겟 분자의 농도를 추론할 수 있게 된다.

이러한 프로브-타겟 분자간의 결합 과정은 크게 전달 과정과 표면에서의 반응 과정 두 단계로 서술할 수 있다. 이 두 단계 중에서, 용액 내의 타겟 물질의 농도가 낮은 경우에는 주로 타겟 물질의 느린 확산에 의한 전달 과정이 전체 결합 과정의 속도를 제한한다는 것이 잘 알려져 있다.

이렇게 느린 프로브-타겟 분자 결합 속도를 보이는 경우, AC electrokinetics를 활용하여 타겟 물질의 전달 속도를 향상시킬 수 있다. AC electroosmosis, dielectrophoresis, AC 그리고 electrothermal flow 등의 방법이 최근에 각광을 받고 있다. 그 중에서도, AC electrothermal flow는 피나 혈청과 같이 전도도가 비교적 높은 생물학적 수용액 환경에서도 효과적으로 적용될 수 있다는 장점을 가진다.

본 논문은 AC electrothermal flow를 활용하여 바이오 센서의 성능을 향상시키는 방안을 제안한다. 동심원 구조를 갖는 바이오센서 소자를 기반으로 한 시뮬레이션 결과는 AC electrothermal flow를 유도하였을 때 타겟 물질이 센서 표면으로 더 빠르게 전달되어 전체적인 프로브-타겟 결합 속도를 향상시킬 수 있음을 보여준다. 또한, AC electrothermal flow의 효과에 대한 실험적인 검증을 위해 급성 심근 경색증의 지표물질인 cardiac troponin-I 검출하는 실험을 진행하였다. 탄소나노튜브 네트워크

기반의 바이오센서에 AC 전압을 인가하여 AC electrothermal flow를 발생시킬 경우, 프로브-타겟 간의 결합으로 인해 발생하는 전기적 신호의 변화 속도가 증가하고 그에 따라 센서가 전압을 인가하지 않은 경우에 비해 훨씬 향상된 성능을 보임을 확인하였다.

주요어: Biosensor, Carbon nanotube, AC electrothermal flow, Cardiac troponin I (cTnI)

학번: 2015-20971